polymers

MDPI

Article

Modification of the Structure and Linear/Nonlinear Optical Characteristics of PVA/Chitosan Blend through CuO Doping for Eco-Friendly Applications

Sami S. Alharthi and Ali Badawi *

Department of Physics, College of Science, Taif University, P.O. Box 11099, Taif 21944, Saudi Arabia
* Correspondence: daraghmeh@tu.edu.sa; Tel.: +966-543-414-808

Abstract: The solution casting technique is utilized to fabricate blank and CuO-doped polyvinyl alcohol/chitosan (PVA/CS) blends for eco-friendly applications. The structure and surface morphologies of prepared samples were explored by Fourier transform infrared (FT-IR) spectrophotometry and scanning electron microscopy (SEM), respectively. FT-IR analysis reveals the incorporation of CuO particles within the PVA/CS structure. SEM analysis exposes the well-dispersion of CuO particles in the host medium. The linear/nonlinear optical characteristics were found on the basis of UV-visible-NIR measurements. The transmittance of the PVA/CS decreases upon CuO increasing to 20.0 wt%. The optical bandgap ($E_{g\ dir.}/E_{g\ ind.}$) decreases from 5.38/4.67 eV (blank PVA/CS) to 3.72/3.12 eV (20.0 wt% CuO-PVA/CS). An obvious improvement in the optical constants of the PVA/CS blend is achieved by CuO doping. The Wemple-DiDomenico (WDD) and Sellmeier oscillator models were utilized to examine the CuO role dispersion behavior of the PVA/CS blend. The optical analysis shows clear enrichment of the optical parameters of the PVA/CS host. The novel findings in the current study nominate CuO-doped PVA/CS films for applications in linear/nonlinear optical devices.

Keywords: polyvinyl alcohol/chitosan blend; CuO doping; linear/nonlinear optical; optical bandgap; Wemple-DiDomenico model; eco-friendly applications

Citation: Alharthi, S.S.; Badawi, A. Modification of the Structure and Linear/Nonlinear Optical Characteristics of PVA/Chitosan Blend through CuO Doping for Eco-Friendly Applications. *Polymers* **2023**, *15*, 2391. https://doi.org/10.3390/polym15102391

Academic Editor: Andrea Ehrmann

Received: 20 April 2023
Revised: 5 May 2023
Accepted: 15 May 2023
Published: 20 May 2023

1. Introduction

Polymeric composites have received great attention because of their effective role in various applications, including the industrial, biological, medical, shielding and entertainment fields [1–5]. Polyvinyl alcohol (PVA), polyvinyl pyrrolidone (PVP), chitosan (CS), carboxymethyl cellulose (CMC) and polyethylene glycol (PEG) possess many attractive features over the rest of polymers, such as non-toxicity, water-solubility, bio-compatibility, eco-friendly and degradability [6–8]. Polymeric composites (PCs) are mainly produced by doping small amounts of fillers in a host polymeric matrix for such an application while blending two polymers or more is another scientific trend to yield new polymeric hosts with specific characteristics for updated applications. Particularly, PVA and CS polymers could be blended to produce a novel polymeric host for a lot of applications. PVA possesses high transmittance Vis/NIR regions and a broad bandgap (5.40 eV). Moreover, the hydroxyl groups (—OH) attached to its carbon-chain backbone perform as a hydrogen bonding source that enhances the complexation process [9], while CS, as chitin's derivative, is the most available polymer that exists in nature [10]. CS could play a dominant role in medical issues because of its unique biocompatibility, antifungal and antimicrobial activities [11]. Mixing PVA and CS produces a PVA/CS polymeric blend to serve as a novel host for various kinds of dopants.

Lots of former works related to PCs are found in the literature. For example, the Heiba research group made great progress using CdS/Mg nanostructures (NPs) on the enhancement of optical characteristics of PVA/CMC. The al-Harthi group proved that the

photoluminescent and optical behavior of the PVP/PVA blend could be tailored by incorporating with non-stoichiometric SnS [12]. The microstructure of the PVA/CMC/graphene oxide blend was modified via doping with Fe_3O_4 NPs for energy storage issues by Alsulami and Rajeh [13]. Moreover, the optical constants of the PVA/CS blend were enhanced by filling it with graphene/Fe_2O_3 for energy storage applications [14]. The Pashameah group concluded that the electrical performance of PVA/CMC was enhanced by MnO_2 incorporation for optoelectronic applications [15]. The Norouzi research group showed that a PVA/CS blend adapted with TiO_2/graphene oxide or carbon quantum dots could improve wound healing [16]. Similarly, Venkataprasanna et al. concluded that a CuO-filled CS/PVA/graphene oxide blend could be effectively applied for wound healing [17]. Furthermore, the storage modulus and glass transition temperature of CS were greatly enhanced by Fe_2O_3 NPs.

This work focuses on the enhancement of microstructure and linear/nonlinear optical performance of PVA/CS via CuO doping for eco-friendly applications. Copper oxide is preferred as a filler in the PVA/CS blend because of its non-toxicity, abundance, low cost, chemical stability and environmental friendliness. Moreover, its biocompatibility and high antibacterial activities qualify CuO PCs for a lot of medical and daily applications. In addition, CuO's relatively small optical bandgap (1.2 eV) and large optical absorption coefficient could play a potential role as a filler for LEDs, solar cells, energy storage and other optoelectronic applications. For that, different CuO contents doped in PVA/CS blend were prepared with the solution casting method. The modification in PVA/CS blend structure due to CuO doping was examined by a Fourier transforms infrared (FT-IR) spectrophotometer. The surface morphology was investigated using scanning electron microscopy. Linear/nonlinear optical constants have been investigated based on UV/Vis/NIR data. The obtained investigations reveal the suitability of CuO-doped PVA/CS films for various linear/nonlinear optical applications such as LEDs, fast communications and energy storage devices.

2. Methods and Materials

Solution casting technique presented in the literature was carried out to fabricate different contents (0.5, 1.0, 5.0, 10.0 and 20.0 wt%) of CuO-doped PVA/CS polymeric blends. To perform the process, starting sources of PVA (M. W.: 85,000 g·mol^{-1}), chitosan (CS) in powder form (≥75% deacetylated) and copper oxide (CuO; purity > 99.0%) were obtained from Sigma-Aldrich Co. (St. Louis, MO, USA). First, at 70 °C, 7.5 PVA grams were dissolved in 250 mL of double distilled water (DDW) for 4 h. In parallel, 2.5 CS grams were dissolved in acetic acid/DDW/(1:9) at 25 °C for 24 h. Both solutions were mixed for 4 h until a homogenous PVA/CS blend (3:1) was achieved. Next, certain amounts of CuO powder were blended to prepare CuO-doped PVA/CS blends. Afterward, the different CuO-PVA/CS blends were cast in Petri dishes for one day at 55 °C. Next, the samples were peeled out and marked by C_0 (blank blend) to $C_{20.0}$ (20.0 wt% of CuO-PVA/CS blend). A digital micrometer was used to measure films' thickness and found 0.18 ± 0.01 mm.

Films' surface morphology was investigated using a scanning electron microscope (JSE-6390LA, JEOL Ltd., Tokyo, Japan). Absorption bands and structures' changes were explored at room temperature (RT) using FT-IR (Shimadzu, IRAffinity-1S, Kyoto, Japan) spectrophotometer with the KBr pellets technique. UV-visible-NIR measurements were recorded at RT using a spectrophotometer (JASCO V670, Jasco Corp., Easton, MD, USA). Tauc's technique was applied to investigate both direct/indirect bandgap (E_g) values as follows [6,18]:

$$(\alpha h\nu)^m = B\left(h\nu - E_g\right) \quad (1)$$

where $\alpha (= \frac{1}{d}\ln\frac{1}{T}$ [6]), and d are optical absorption coefficient and films' thickness, B is constant and m is a parameter that may take 2 and 1/2 values for allowed direct/indirect electronic transitions [18,19].

Localized states and created defects' role in host's bandgap as a result of CuO doping is investigated via the determination of the Urbach energy (E_u) as follows [13]:

$$\alpha = \alpha_0 \exp(h\nu / E_u) \tag{2}$$

where α_0 is a constant.

The refractive index (n), extinction coefficient (K), and optical conductivity ($\sigma_{opt.}$) in UV/Vis/NIR regions were calculated as

$$n = \left(\frac{1+R}{1-R}\right) + \left[\frac{4R}{(1-R)^2} - K^2\right]^{1/2} \tag{3}$$

$$K = \frac{\alpha\lambda}{4\pi} \tag{4}$$

$$\sigma_{opt.} = \frac{\alpha n C}{4\pi} \tag{5}$$

where C is light speed, R is reflectance, and λ is photons/wavelength.

The dielectric permittivity constants (real ε_r, imaginary ε_i) and surface/volume energy loss functions (SELF/VELF) were also determined from [20,21]:

$$\varepsilon_r = n^2 - K^2 \tag{6}$$

$$\varepsilon_i = 2nK \tag{7}$$

$$SELF = \frac{\varepsilon_i}{(\varepsilon_r + 1)^2 + \varepsilon_i^2} \tag{8}$$

$$VELF = \frac{\varepsilon_i}{\varepsilon_r^2 + \varepsilon_i^2} \tag{9}$$

Moreover, Wemple-DiDomenico (WDD) model was followed to examine n dispersion [22], whereas Sellmeier oscillator relations were applied to investigate the rest of the optical parameters as infinite refractive index (n_∞), average oscillator strength (S_0), average inter-band oscillator wavelength (λ_0), infinite dielectric parameter (ε_∞), lattice dielectric parameter (ε_L) and free carrier concentration/effective mass (N/m^*) as [23,24]:

$$n^2 = 1 + \frac{E_d E_0}{E_0^2 - (h\nu)^2} \tag{10}$$

$$\frac{n_\infty^2 - 1}{n^2 - 1} = 1 - \left(\frac{\lambda_0}{\lambda}\right)^2 \tag{11}$$

$$\left(n^2 - 1\right)^{-1} = \frac{1 - \left(\frac{\lambda_0}{\lambda}\right)^2}{S_0 \lambda_0^2} \tag{12}$$

$$S_0 = \frac{n_\infty^2 - 1}{\lambda_0^2} \tag{13}$$

$$\varepsilon_\infty = n_\infty^2 \tag{14}$$

$$\varepsilon_r = n^2 = \varepsilon_L - \frac{e^2}{4\pi^2 C^2 \varepsilon_0} \frac{N}{m^*} \lambda^2 \tag{15}$$

where e is free electron charge, and ε_0 is space dielectric constant.

The linear first-order susceptibility ($\chi^{(1)}$), nonlinear third-order susceptibility ($\chi^{(3)}$) and nonlinear refractive index (n_2) were investigated as [25,26]

$$\chi^{(1)} = \frac{n^2 - 1}{4\pi} \tag{16}$$

$$\chi^{(3)} = 1.7 \times 10^{-10} \left(\chi^{(1)}\right)^4 \tag{17}$$

$$n_2 = \frac{12\pi}{n}\chi^{(3)} \tag{18}$$

3. Results and Discussion

3.1. Morphological Analysis

Films' surface morphologies were captured by a scanning electron microscope (SEM). Figure 1a–f illustrates SEM micrograms of the blank and different (0.5 to 20 wt%) CuO-PVA/CS films, respectively. The SEM microgram of the blank film is spot-free with a smooth surface (Figure 1a), whereas distinguishable bright spots related to the CuO granules are clearly noticed in SEM micrographs of 0.5 and 1.0 wt% of CuO-PVA/CS films. These spots become denser, closer and more compact as the CuO concentration is increased to 20 wt%.

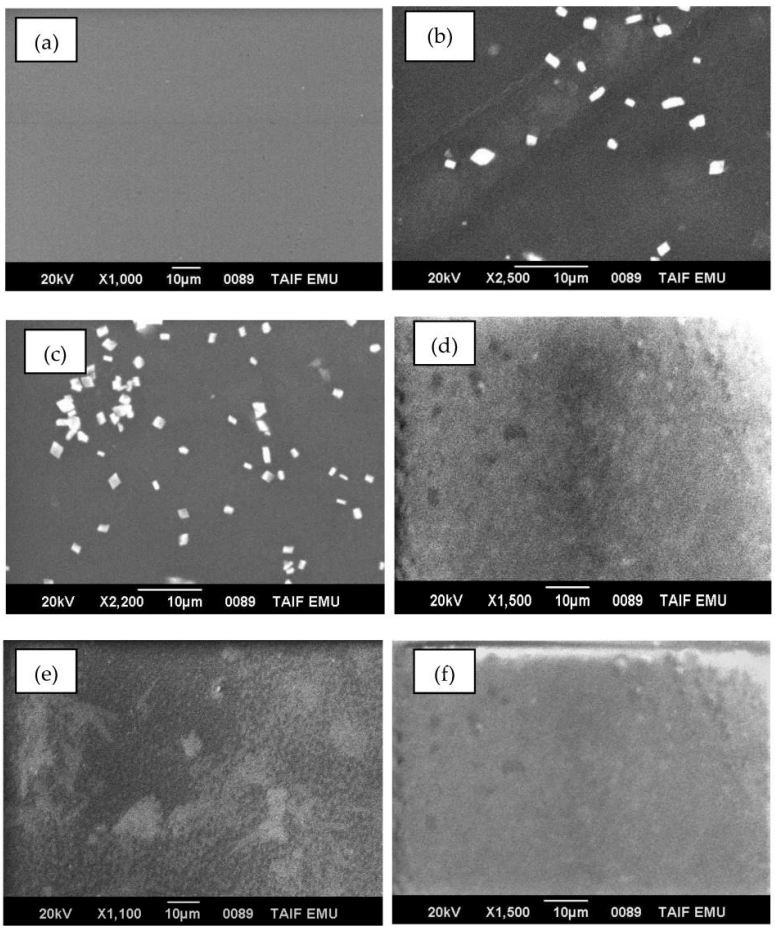

Figure 1. SEM micrograms of (**a**) blank and (**b**–**f**) different (0.5 to 20 wt%) CuO-PVA/CS films.

3.2. FT-IR Analysis

Figure 2a,b depicts FT-IR transmittance spectra of blank and different CuO-PVA/CS films in the 400 to 4000 cm^{-1} range, as demonstrated by plots, clear variations in intensity and sites of dominant absorption bands of doped samples with respect to the blank one.

These changes confirm the interactions between the CuO molecules with the structure of the host PVA/CS matrix. This interaction mainly takes place by replacing the OH groups in the host structure with that of the CuO ones [27]. Relative to FT-IR spectra of blank PVA/CS film and pure CuO material, the main absorption bands and vibrations are recorded (Table 1). Similar FT-IR performance is noticed in the CuO-PVA/CS films with clear intensity variations and slight location shifts with broadening in the absorption bands. These changes are pronounced in the regions 3900–3600 cm^{-1} and 1300–400 cm^{-1} as background shadows in Figure 1a, whereas the absorption bands correspond to the Cu-O bonds may overlap with those of the host matrix at the 1300–400 cm^{-1} region, as shown in Figure 1b. Our findings reveal the complete incorporation of CuO and the host medium. The same trends are reported in the literature [27–29].

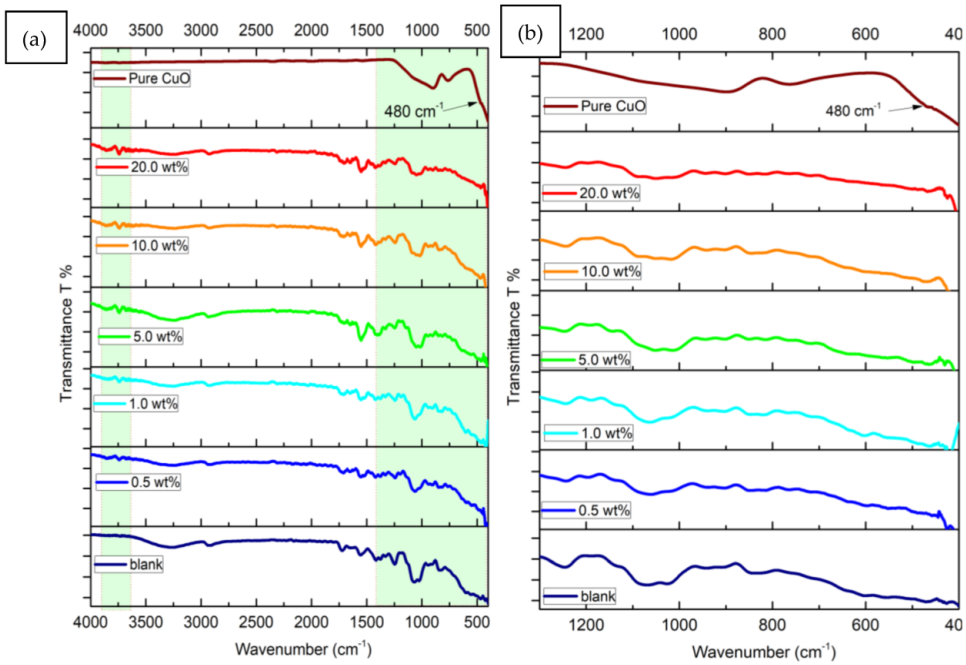

Figure 2. FT-IR spectra (**a**) full wavelength range and (**b**) 1300–400 cm^{-1} of blank and CuO-PVA/CS films.

Table 1. FT-IR absorption bands and bonds' vibration.

Wavenumber Site (cm^{-1})	Bond Vibration	References
3280	O—H stretching	[30,31]
2915	C—H asymmetric stretching	[13,32]
1724	C=O stretching	[30,33]
1552	O—H and C—H bending	[34]
1423	C—H bending	[33,35]
1251	C—H wagging	[33,34]
1069	C—O bending	[27,28]
832	C—C stretching	[34,36]
435	O—H wagging, C—C bending and CuO	[29,33,37]
891	Cu—O—Cu stretching	[38,39]
762	Cu—O stretching	[38,40]
480	Cu—O stretching	[41]

3.3. UV/Vis/NIR Investigations

The effect of CuO concentration on the optical parameters of the PVA/CS blend has been explored on the basis of the UV/Vis/NIR measurements. The wavelength dependence of the transmittance (T) and absorbance (A) of blank and different CuO contents filled PVA/CS blends are presented in Figure 3a,b, respectively. It is noticed that at any certain λ, T decreases in visible-NIR regions as the CuO content is increased from 0 to 20 wt%. For example, the T of the blank PVA/CS film is more than 80% in the visible region, while it

decreases to about 3% for 20 wt% of CuO-PVA/CS film in the same region. Moreover, as the CuO content is increased from 0 to 20 wt%, the UV cut-off edge is red-shifted to longer wavelengths from 225 nm to 358 nm. This valuable result nominates the possible role of CuO-PVA/CS films in UV-shielding applications. In contrast, the absorption increases due to the increase of CuO contents. In addition, clear redshifts in the absorption edges are noticed. Furthermore, two absorption peaks at 211 nm and 258 nm are detected in all absorption spectra that correspond to the PVA electronic $\pi \rightarrow \pi^*$ transitions [42], whereas the absorption edge detected at 324 nm refers to the electronic $n \rightarrow \pi^*$ transitions [43]. The decrease in the optical transmittance and hence increment in the absorption amounts due to CuO doping is attributed to the increase in defects (shown below), which leads to a decrease in the optical band gap of the PVA/CS blend, as discussed in Figure 4.

Based on Tauc's equation (Equation (1)), direct/indirect optical bandgap ($E_{g\ dir.}/E_{g\ ind.}$) of blank and CuO-PVA/CS films has been obtained from $(\alpha h\nu)^2$ and $(\alpha h\nu)^{1/2}$ curves vs. $h\nu$, respectively, as depicted (Figure 4). The x-axis intercepts of extrapolated linear parts of these curves to $h\nu = 0$ equal E_g values as listed in Table 2. The obtained $E_{g\ dir.}/E_{g\ ind.}$ values of blank PVA/CS film are 5.38 eV and 4.67 eV. These values are well-consistent with the reported ones [34,44]. The $E_{g\ dir.}/E_{g\ ind.}$ values of CuO-PVA/CS films decrease to 3.72 eV and 3.12 eV as CuO concentration is upraised to 20 wt%. Moreover, it is clear that both 0.5 wt% and 1.0 wt% CuO-PVA/CS films possess second bandgap values of 4.79 eV and 4.57 eV, respectively, as illustrated in Figure 4a. This finding reveals that the absorption happens as a result of charge transfer between two different energy levels. The first transition occurs between the molecular orbits of the host matrix, while the other electronic transition takes place between the created energy state due to CuO particles and those of the host matrix. Similar findings were recorded in previous works [21,45]. So, the E_g narrowing mainly results due to localized states and defects created between the highest occupied molecular orbital (HOMO) and lowest unoccupied molecular orbital (LUMO) of the PVA/CS blend due to CuO doping [42,46]. Similarly, Heiba et al. concluded that 4 wt% of $Cd_{0.9}Mg_{0.1}S$ nanofillers led to a reduction in the E_g of PVA/CMC blend from 5.4 eV to 5.02 eV [44]. Additionally, the E_g of the PVA/CMC/GO blend was reduced to 3.34 eV using 1.0 wt% of Fe_3O_4 doping [13]. Formerly, we modified the optical bandgap of PVA/Gr from 5.38 eV to 4.78 eV by Fe_2O_3 doping [47].

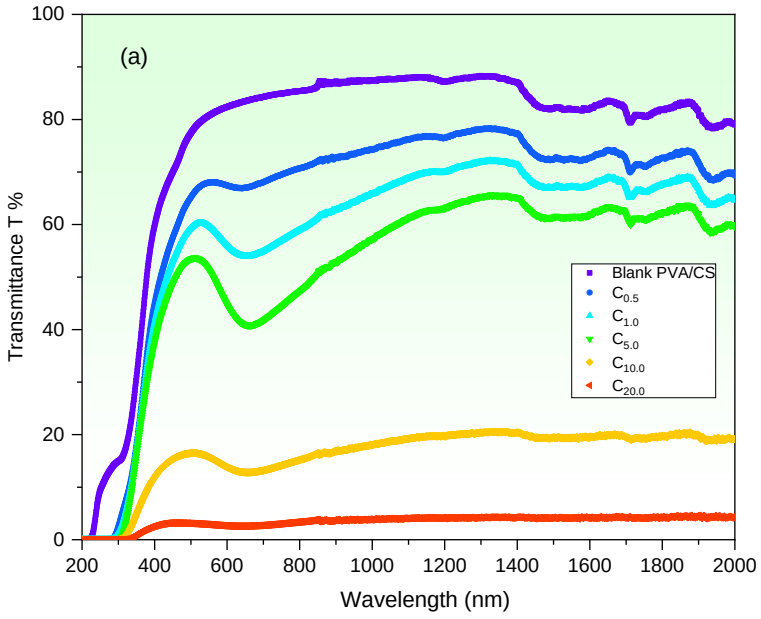

Figure 3. *Cont.*

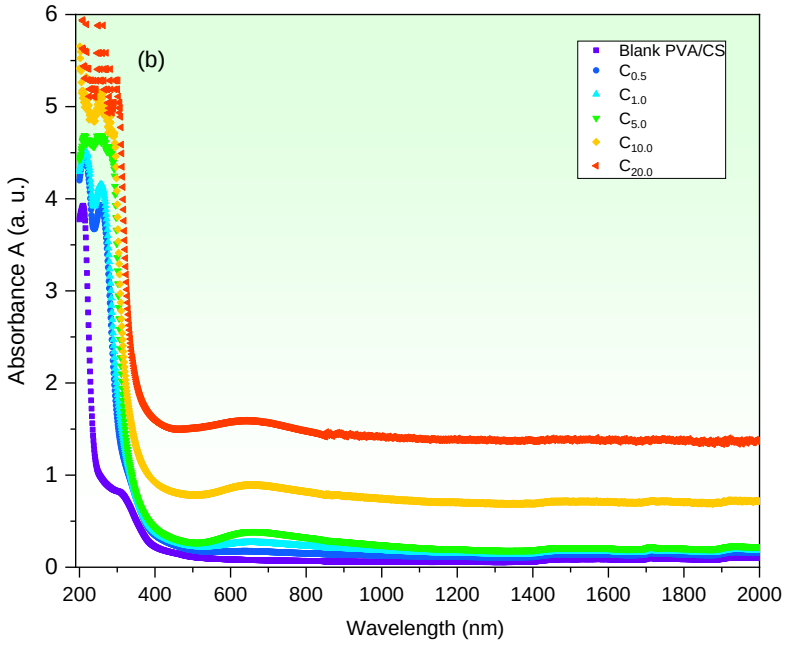

Figure 3. (**a**) Wavelength dependence of the transmittance (T) and (**b**) absorbance (A) spectra of blank and different CuO-PVA/CS films.

Table 2. Direct/indirect bandgap, Urbach energy and refractive index of CuO-PVA/CS films.

CuO wt%	Direct $E_{g\ dir.}$ (eV)	Indirect $E_{g\ ind.}$ (eV)	*Eu* (eV)	*n* @ 650 nm
0	5.38	4.67	0.48	1.20
0.5	4.21	3.45	0.52	1.31
1.0	4.13	3.38	0.60	1.39
5.0	3.97	3.29	0.69	1.49
10.0	3.90	3.22	1.24	1.83
20.0	3.72	3.12	1.79	2.25

The defects and localized energy states created in CuO-PVA/CS films could be proved by investigating the Urbach energy (E_u) (Equation (2)). It shows the exponential dependence of the absorption coefficient and photons energy ($h\nu$). E_u is estimated (Table 2) by plotting $ln\alpha$ vs. $h\nu$, as illustrated in Figure 5. It was noticed that E_u grows from 0.48 eV (blank PVA/CS) to 1.79 eV (20 wt% CuO-PVA/CS). The increase in E_u indicates the growth of localized states and defects that works as trapping centers in the forbidden region of the PVA/CS host [48]. Similar evidence is reported in the literature [13,25,49]. As an original result, the optical bandgap of PVA/CS is tailored by CuO doping for a lot of optical and environmental applications.

The optical performance of such material is mainly established by investigating the refractive index (n* = n-i*K*) to dictate its applications. The real (n) and imaginary (*K*) parts describe the dispersion behavior of the electromagnetic wave within the material. Both *n* and *K* at the swept wavelength (λ) are calculated using Equations (3) and (4), respectively. The wavelength dependence of *n* and *K* of blank and CuO-PVA/CS films are illustrated in Figure 6a,b, respectively. According to Figure 6a, it is noted that *n* follows the absorbance performance (Figure 3b). In other words, *n* decreases steeply upon raising λ in the UV region, whereas it remains semi-steady in Vis/NIR regions. Moreover, it is seen that the *n* of PVA/CS is enhanced as a result of CuO doping, which proposes it for updated applications in optical and optoelectronic devices. For instance, *n* increases from 1.2 (blank PVA/CS) to 2.25 (20 wt% CuO-PVA/CS) at 650 nm. The improvement in the *n* value refers to the growth in the films' density and intermolecular bonds due to CuO doping [27,50,51], whereas *n* remains quasi-steadily in low photons energy due to films' restricted absorbance in this

region, whereas, according to Figure 6b, K declines with increasing λ in the UV region, whereas it increases gradually in visible-NIR regions. Furthermore, K increases as the CuO content is increased. These findings could be understood on the basis of the increment of the dispersion as a result of the reflectance increase due to defects' growth [51].

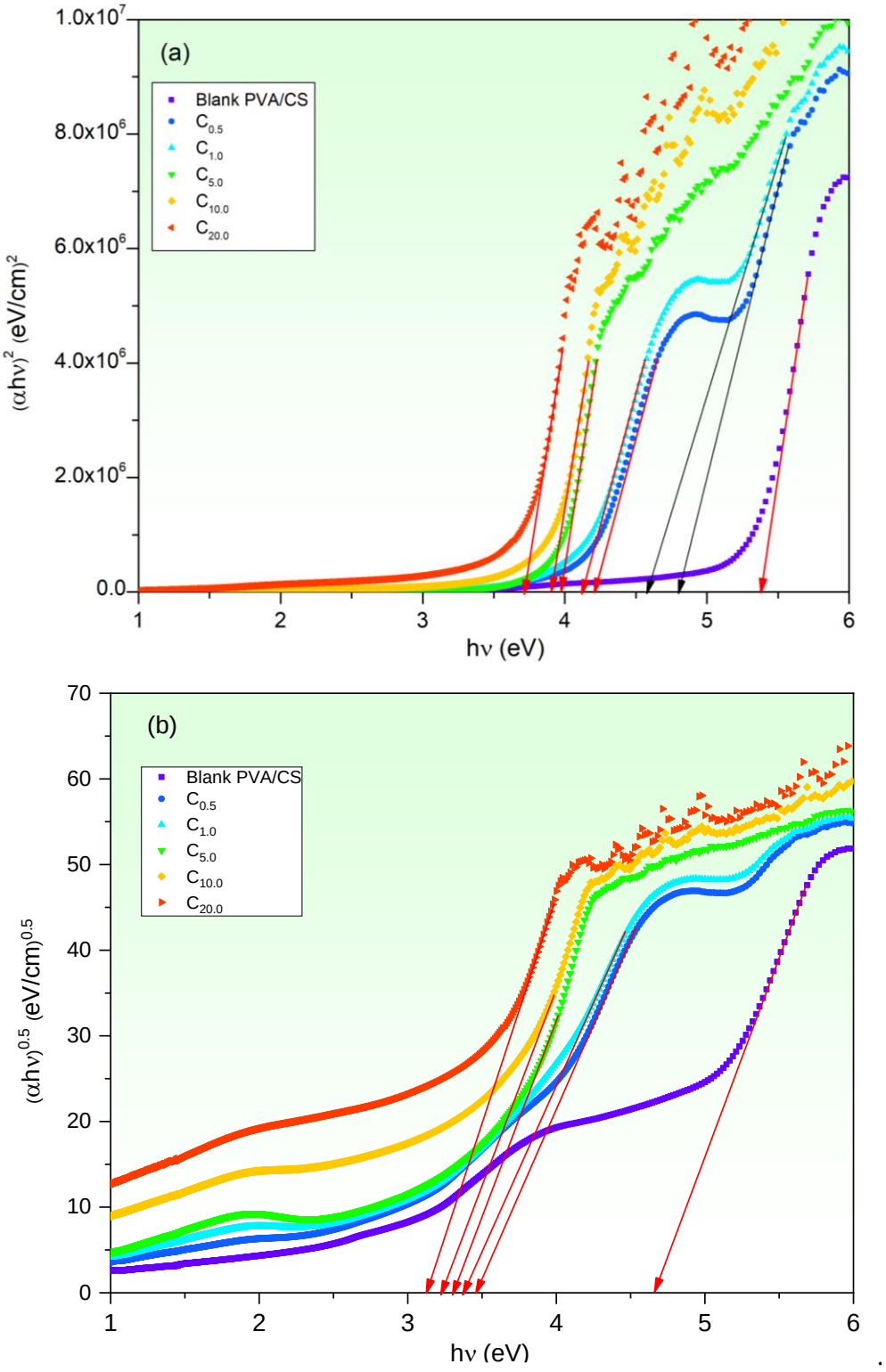

Figure 4. Tauc's plots (**a**) direct and (**b**) indirect status of CuO-PVA/CS films.

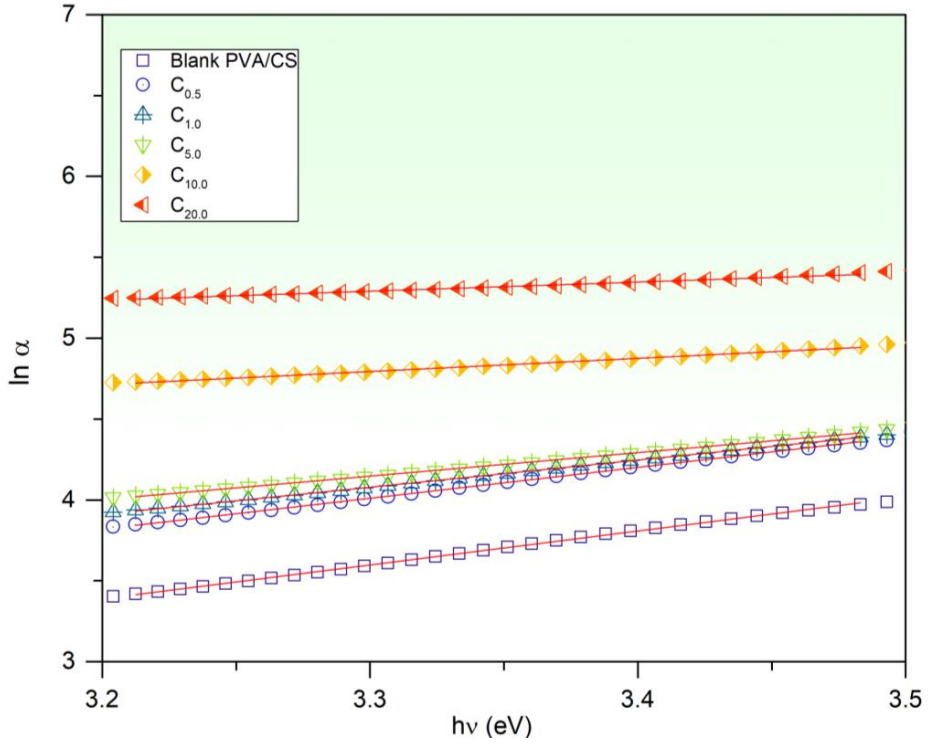

Figure 5. *lnα* vs. *hν* of CuO-PVA/CS films.

Based on the absorption coefficient α and n, $\sigma_{opt.}$ of CuO-PVA/CS samples was determined (Equation (5)) and illustrated in Figure 7. It is observed that $\sigma_{opt.}$ of the films behaves in a similar way to the optical absorbance (Figure 3b). As λ is red-shifted to longer values in the UV region, $\sigma_{opt.}$ decreases steeply, while it behaves steadily in the Vis/NIR regions. In contrast, $\sigma_{opt.}$ increases upon increasing the CuO content in the PVA/CS host. For example, at 650 nm, $\sigma_{opt.}$ enhances from 2.56×10^{10} s^{-1} (blank PVA/CS) to 9.85×10^{10} s^{-1} (20 wt CuO-PVA/CS). The $\sigma_{opt.}$ enhancement is understood on the basis of the increment in created electrons as a result of the absorption increase of the incident photons [27,52]. The increase in absorption is also reinforced by the growth in the defects, as discussed in E_u findings. These findings are very consistent with reported data [21,53,54]. Shamekh et al. proved that $\sigma_{opt.}$ of PVA was pronouncedly enhanced by MgO doping.

The dielectric parameters (ε_r and ε_i), together with the surface/volume energy loss functions (SELF/VELF) of the blank and CuO-PVA/CS films, have been determined. These constants are investigated to nominate their possible participation in many fields as superconductors and energy storage devices. ε_r associates with traveling wave dispersions within such material, while ε_i relates to the dissipated energy rate through their propagation [21]. ε_r, ε_i, SELF and VELF were calculated by Equations (6) to (9) and presented in Figure 8a–d, respectively. According to ε_r spectra (Figure 8a), it follows the refractive index n performance. ε_r decreases steeply as λ is red-shifted in the UV region, whereas it remains semi-constant in the visible-NIR regions. Furthermore, ε_r rises as CuO content is increased to 20 wt%. For example, ε_r enhanced from 1.43 (blank PVA/CS) to 5.08 (20 wt% CuO-PVA/CS) at λ = 650 nm. The enhancement in ε_r results due to the increase in the dispersion as a result of a defects increase (Urbach energy findings). On the other hand, the imaginary part ε_i of the film performs similarly to the extinction coefficient K (Figure 6b). ε_i decreases greatly as λ increases in the UV region, while it increases slowly in Vis/NIR region for small CuO contents ($\leq$5 wt%) and increases pronouncedly for the high CuO contents (10 and 20 wt%). Moreover, ε_i increases as the CuO content is raised. This behavior refers to polarization and dipole motion fluctuations [26,55,56]. Similar findings are reported in the literature [26,57,58]. Moreover, it is noticed that SELF and VELF spectra perform in a similar way. Both SELF and VELF values increase noticeably as λ is red-shifted

to longer wavelengths in the Vis/NIR regions. Moreover, it is noted that at any λ, the VELF value is larger than the SELF value, which indicates that the energy loss by the traveling electrons within the films due to the doped CuO particles is larger than those traveling on their surfaces. In addition, both SELF and VELF increased upon increasing the CuO contents. This increment in SELF and VELF refers to growth in vacant energy levels generated in the host band gap [59]. Similar behavior is noticed El-naggar et al. [26]. They showed SELF and VELF increase of the PVA/PVP upon increasing SnS_2/Fe concentration.

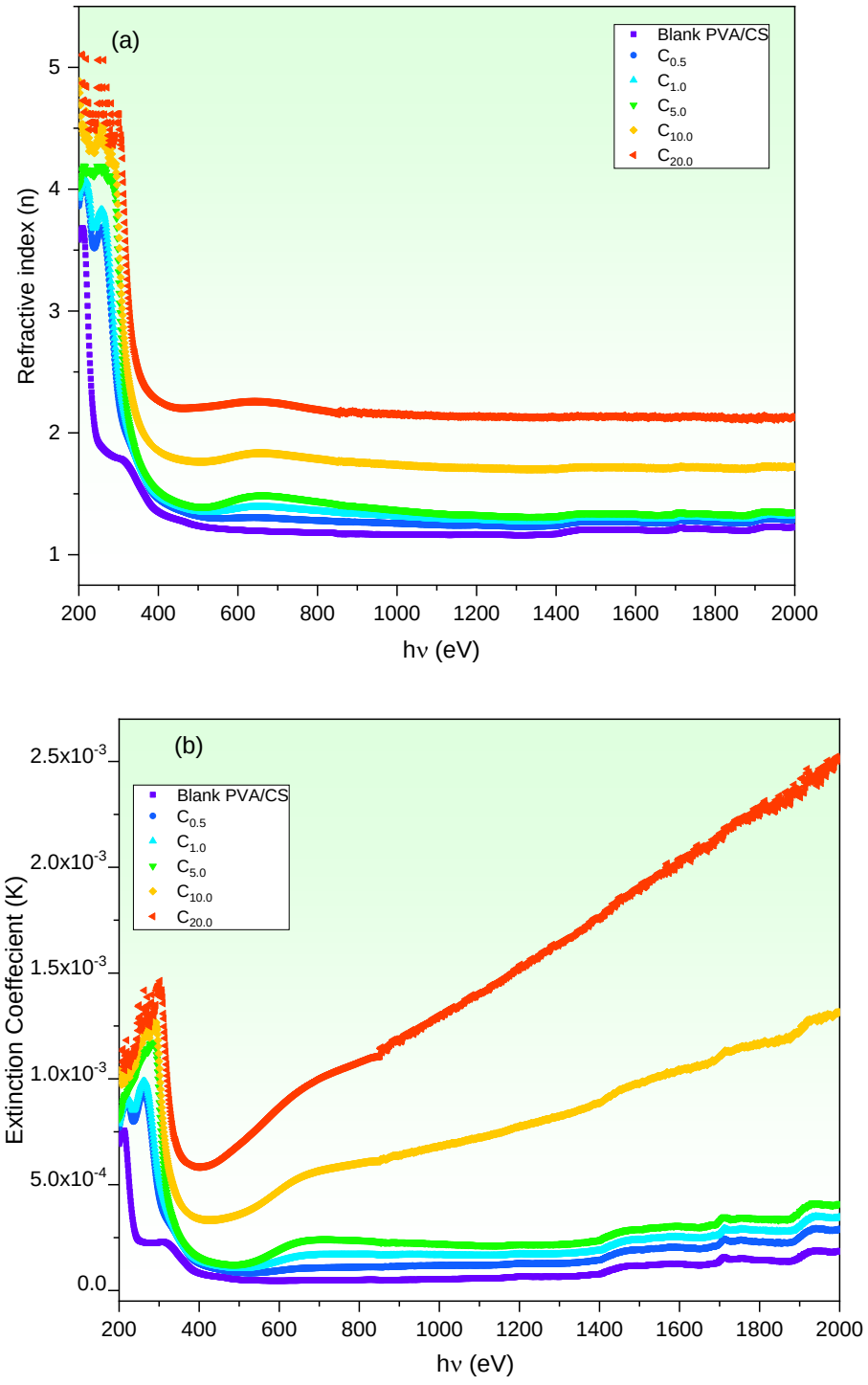

Figure 6. (**a**) *n* and (**b**) *K* vs. wavelength of CuO-PVA/CS films.

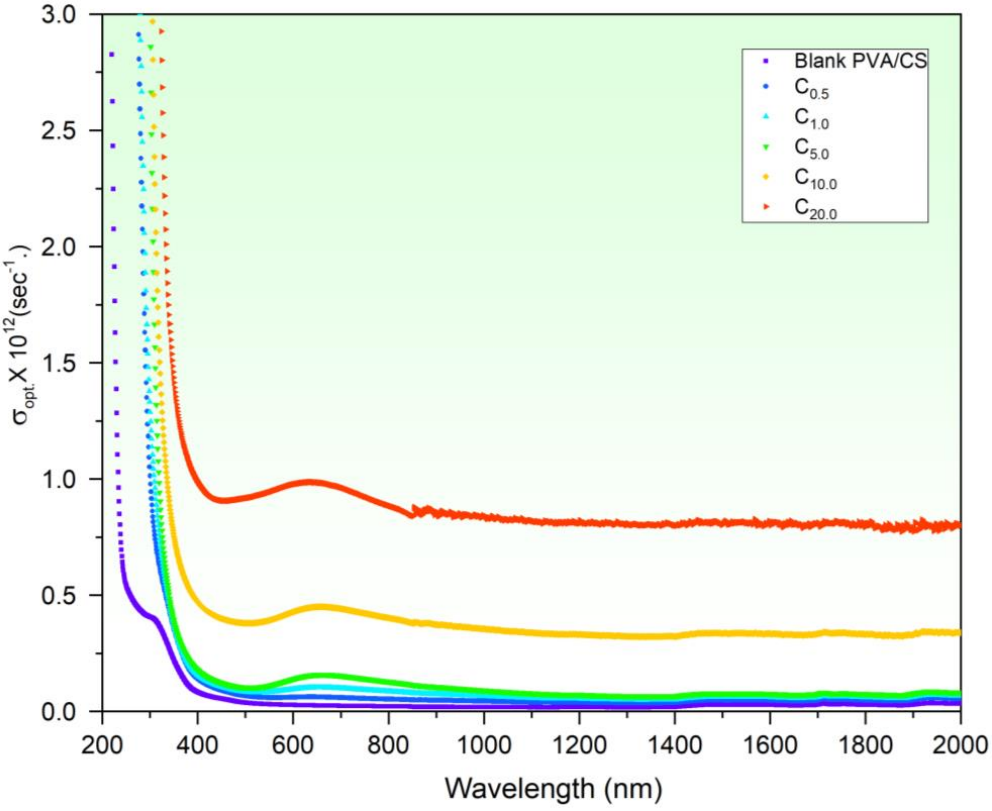

Figure 7. Optical conductivity vs. wavelength of CuO-PVA/CS films.

Moreover, the dispersion parameters of the blank and CuO-PVA/CS films are examined by a single oscillator model (WDD model; Equation (10)) in the normal dispersion region. Investigating E_o and E_d are essential parameters to nominate the applications of the prepared films in communication systems and spectra analysis devices [21]. The values of E_o and E_d are found from $(n^2 - 1)^{-1}$ plots vs. $(h\nu)^2$ as depicted in Figure 9a, where the slopes equal $-1/(E_0E_d)$ and the intersections equal E_0/E_d. Table 3 includes E_o and E_d values. Both E_o and E_d values increase upon increasing the CuO content in the host PVA/CS. This increase in the dispersion energies refers to the increase in the optical transition strength of the system bonds [60].

Table 3. Dispersive parameters of CuO-PVA/CS films.

CuO wt%	E_d (eV)	E_0 (eV)	n_∞	λ_0 (nm)	S_0 (m^{-2})	ε_∞	ε_L	(N/m*) $\times 10^{57}$ ($kg^{-1}.m^{-3}$)
Blank PVA/CS	1.49	4.14	1.16	302.8	3.85×10^{12}	1.35	2.33	4.01
0.5	1.89	4.06	1.21	306.2	5.01×10^{12}	1.47	2.79	5.37
1.0	2.20	4.14	1.24	301.7	5.78×10^{12}	1.53	2.85	5.21
5.0	2.54	4.24	1.26	297.2	6.62×10^{12}	1.58	2.92	5.09
10.0	7.27	4.58	1.55	243.2	2.38×10^{13}	2.41	4.52	7.88
20.0	21.13	6.76	1.98	216.9	6.25×10^{13}	3.94	5.37	8.85

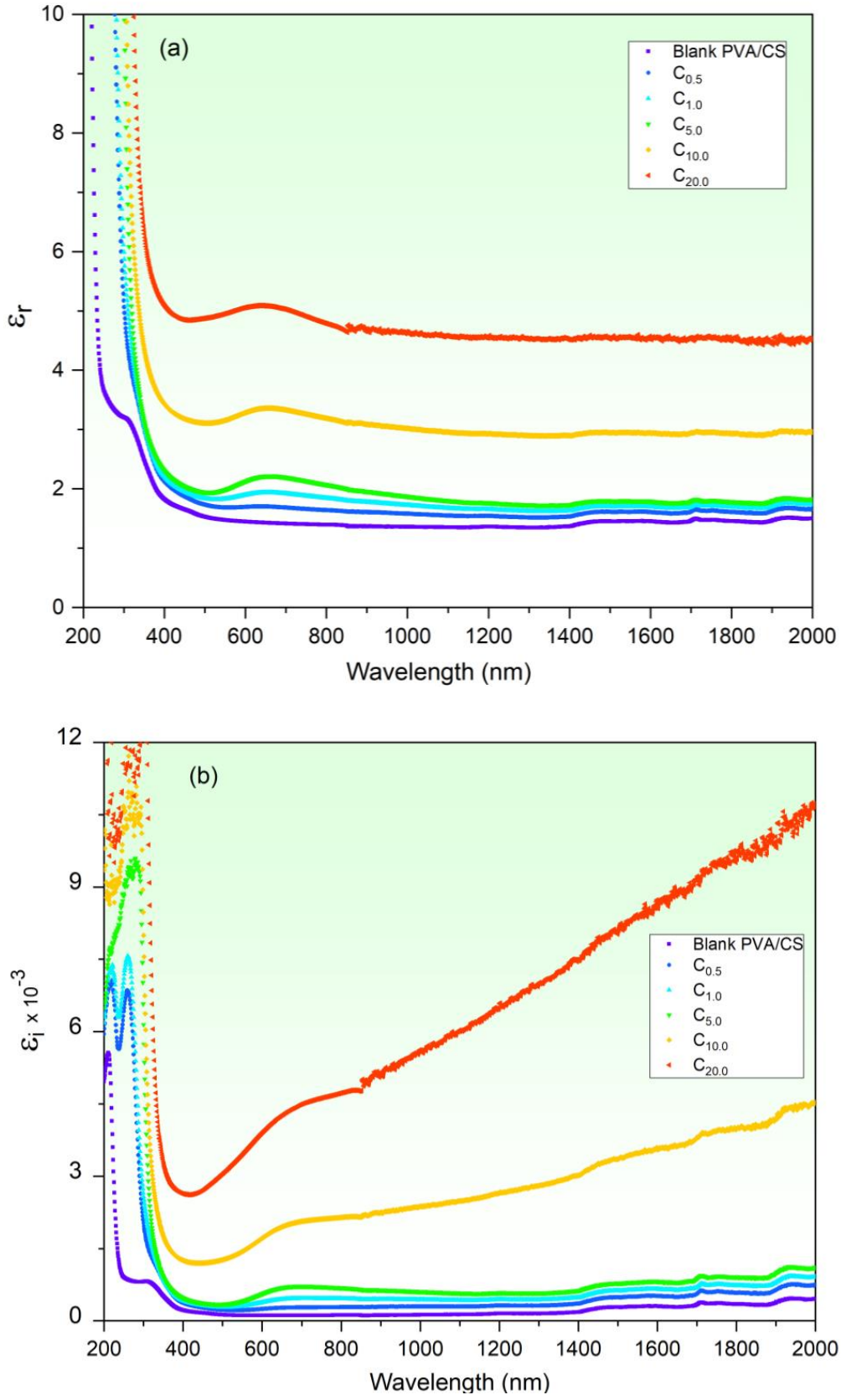

Figure 8. *Cont.*

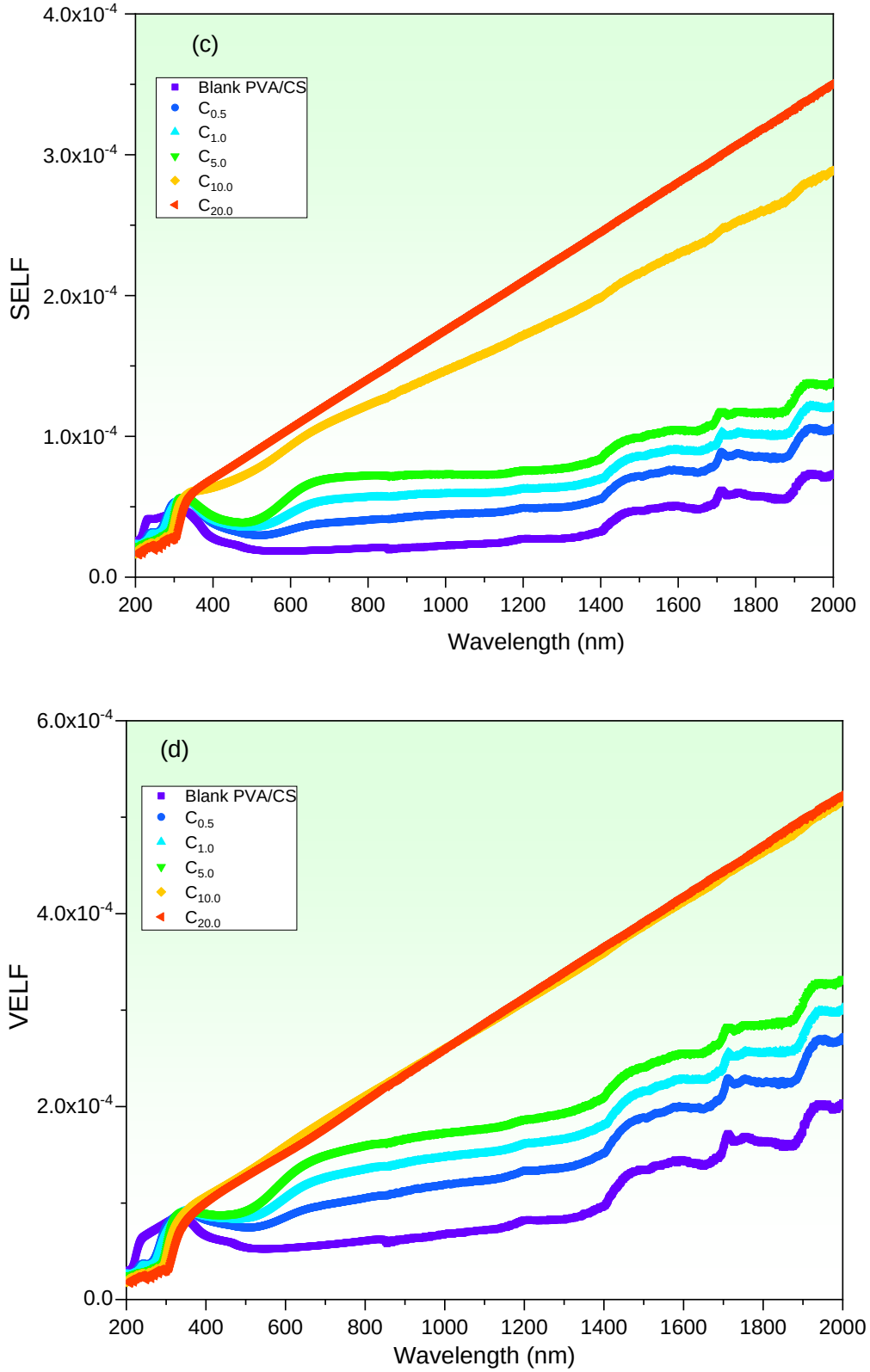

Figure 8. (**a**) Real, (**b**) imaginary dielectric constant. (**c**) SELF and (**d**) VELF of CuO-PVA/CS films.

Furthermore, the infinite refractive index (n_∞), the infinite dielectric constant (ε_∞), and the average oscillator strength (S_0)) of the blank and CuO-PVA/CS films are determined on the basis of the Sellmeier oscillator relations (Equations (11) to (15)). By plotting $(n^2-1)^{-1}$ vs. λ^{-2} (Figure 9b) and equating the slopes with $1/S_0$ and the intersections with

$1/S_0\lambda_0^2$, the values of λ_0, n_∞, S_0 and ε_∞ are obtained and listed in Table 3. While N/m* and ε_L are obtained by plotting n^2 vs. λ^2 (Figure 9c), where the slopes $\left(=\frac{e^2}{4\pi^2C^2\varepsilon_0}\frac{N}{m^*}\right)$ and intersections (=ε_L) as listed in Table 3. It is obvious that all optical behaviors of the PVA/CS blend are altered with CuO doping. For example, ε_∞ of the blank PVA/CS film is greatly enhanced from 1.35 to 3.94 (20 wt% CuO-PVA/CS film). The enhancement in ε_L and ε_∞ refers to the dispersion lattice vibrations as a result of CuO particles [37]. Similar ε_L and ε_∞ findings related to polystyrene filled with manganese (III) chloride were found by Al-Muntaser et al. [37], while N/m* of the blank PVA/CS film is duplicated due to 20 wt% of CuO doping. This result is reasonable as a result of the increment of the free carriers due to CuO doping [21]. Our results are compatible with the literature [61,62].

The nonlinear optical behavior of blank and CuO-PVA/CS samples is explored to recommend their probable applications in nonlinear optical devices. Optical materials with the optical nonlinearity character play an effective role in many applications such as ultrafast lasing switching, frequency converters and telecommunications [21,63]. The nonlinear optical response arises because of the nonlinear polarization that occurs owing to intense electromagnetic wave exposure [21,64,65]. Based on Equations (16) to (18), $\chi^{(1)}$, $\chi^{(3)}$ and n_2 are calculated and presented in Figure 10a–c, respectively. It is noted that $\chi^{(1)}$, $\chi^{(3)}$ and n_2 behave semi-steadily in the Vis/NIR regions, whereas they rise rapidly upon increasing $h\nu$ in the UV region. In addition, as the CuO content is increased to 20 wt%, $\chi^{(1)}$, $\chi^{(3)}$ and n_2 increase noticeably. For instance, at 4.0 eV, $\chi^{(1)}$ of the blank PVA/CS film is enhanced from 0.17 esu to 1.36 esu via 20 wt% CuO doping, while $\chi^{(3)}$ and n_2 of the blank film are enhanced about by three-order of magnitude at the same incident photons energy. These findings are compatible with previous works [25,26,64]. For example, the Ali group found that the nonlinear optical constant of PVA was enhanced pronouncedly by fullerene doping [25]. The obtained nonlinear optical findings of the CuO-PVA/CS films in this study nominate their applications in nonlinear optical devices [65].

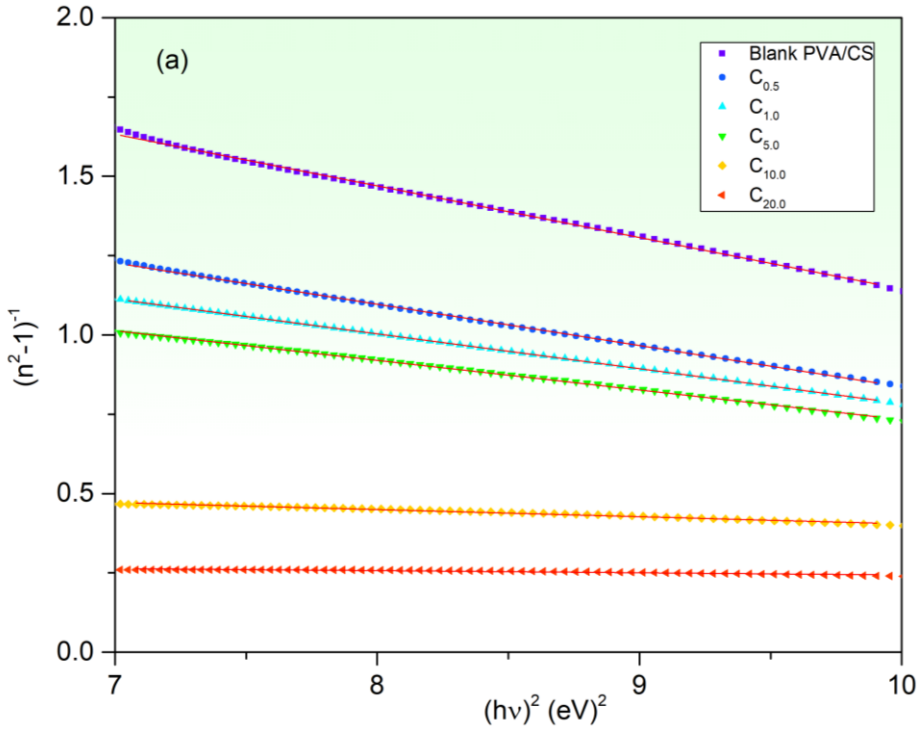

Figure 9. *Cont.*

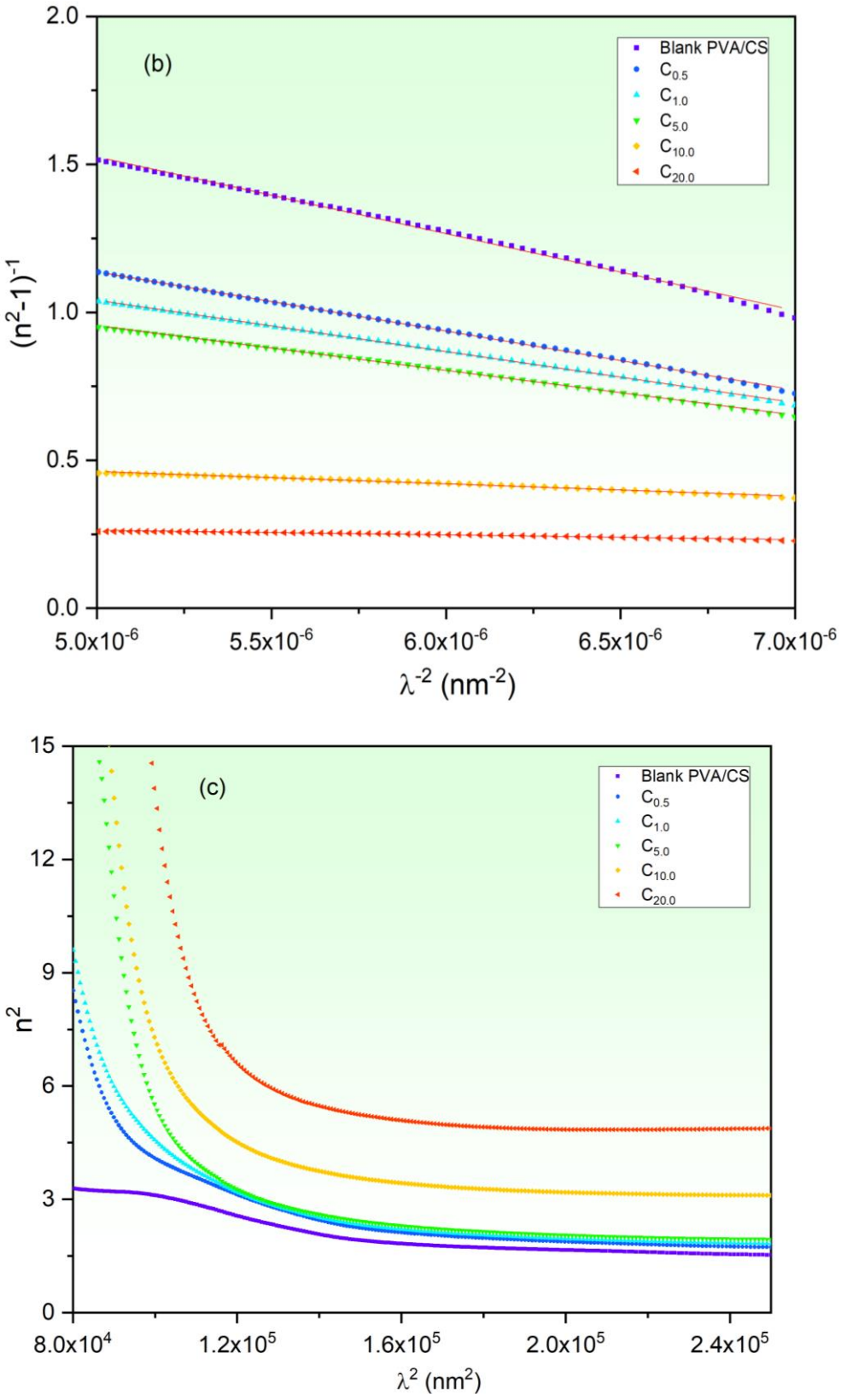

Figure 9. (**a**) $(n^2-1)^{-1}$ vs. $(h\nu)^2$, (**b**) $(n^2-1)^{-1}$ curves vs. λ^{-2} and (**c**) n^2 curves vs. λ^2 of CuO-PVA/CS films.

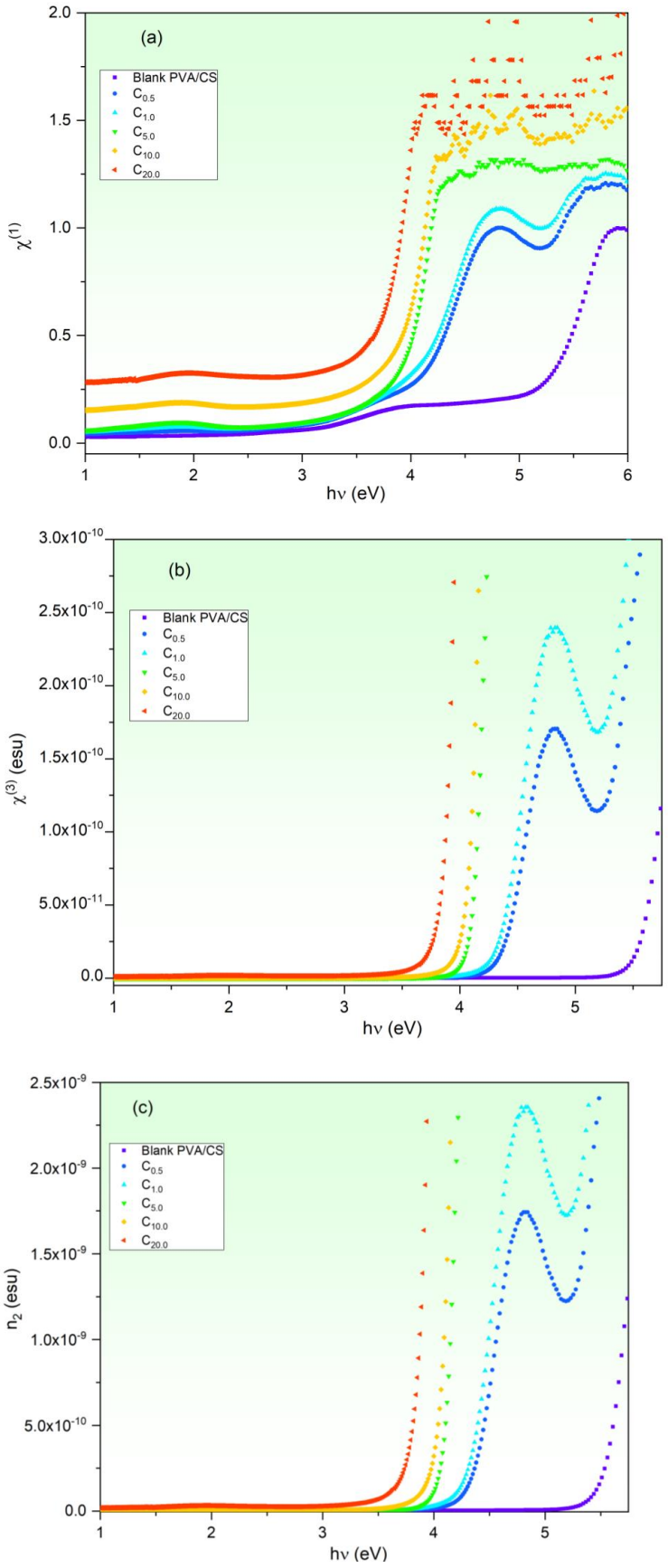

Figure 10. (**a**) First-order susceptibility ($\chi^{(1)}$), (**b**) third-order susceptibility ($\chi^{(3)}$) and (**c**) nonlinear refractive index (n_2) of CuO-PVA/CS films.

4. Conclusions

The solution casting method was followed to fabricate blank and CuO doped in polyvinyl alcohol/chitosan (PVA/CS) blends. The effect of CuO concentrations (0, 0.5, 1.0, 5.0, 10.0 and 20.0 wt%) on PVA/CS structure and linear/nonlinear optical characteristics is discussed in detail. Scanning electron microscope examinations disclose obvious changes in the surface morphologies of PVA/CS film owing to CuO doping. FT-IR measurements prove noticeable modifications in PVA/CS structure due to CuO doping. Noticeable modifications in absorption band's locations and intensities of CuO-PVA/CS films as compared with the blank one. The linear/nonlinear optical parameters were discussed. The transmittance of the PVA/CS blend reduces as a result of CuO increasing to 20.0 wt%. The optical bandgap ($E_{g\ dir.}/E_{g\ ind.}$) decreases from 5.38/4.67 eV (blank PVA/CS) to 3.72/3.12 eV (20.0 wt% CuO-PVA/CS). This decrease in the optical bandgap is interpreted in terms of defects and created states, as verified by Urbach energy investigations. The refractive index, optical conductivity and dielectric constants of PVA/CS are clearly enhanced due to CuO doping, which nominates it for updated applications in optoelectronic devices. The CuO doping role in the dispersion performance of PVA/CS has been investigated using a single oscillator and Sellmeier oscillator relations. For instance, the infinite dielectric constant is greatly enhanced from 1.35 (blank PVA/CS) to 3.94 (20 wt% CuO-PVA/CS film), whereas the concentration of free carriers/effective mass of blank PVA/CS film is duplicated. The nonlinear optical parameters of PVA/CS are also enhanced via CuO doping. $\chi^{(3)}$ and n_2 are improved by about three orders-of-magnitude at 4.0 eV incident photons energy. These novel findings nominate CuO-PVA/CS films for updated optical applications.

Author Contributions: Conceptualization, S.S.A. and A.B.; methodology, S.S.A. and A.B.; software, S.S.A.; writing—original draft preparation, A.B.; writing—review and editing, S.S.A. and A.B.; funding, A.B. All authors have read and agreed to the published version of the manuscript.

Funding: Taif University Researchers Supporting Project number (TURSP-2020/12), Taif University, Taif, Saudi Arabia.

Institutional Review Board Statement: Not applicable.

Data Availability Statement: The data are available on reasonable request from the corresponding author.

Acknowledgments: Authors thank Taif University Researchers Supporting Project number (TURSP-2020/12), Taif University, Taif, Saudi Arabia.

Conflicts of Interest: The authors declare no conflict of interest.

References

1. Prabaharan, M. Chitosan-based nanoparticles for tumor-targeted drug delivery. *Int. J. Biol. Macromol.* **2015**, *72*, 1313–1322. [CrossRef] [PubMed]
2. Khairy, Y.; Mohammed, M.I.; Elsaeedy, H.I.; Yahia, I.S. Optical and electrical properties of SnBr2-doped polyvinyl alcohol (PVA) polymeric solid electrolyte for electronic and optoelectronic applications. *Optik* **2021**, *228*, 166129. [CrossRef]
3. Das, M.; Sethy, P.P.; Singh, U.P.; Sundaray, B. Effect of graphene loadings on electrical properties of polyaniline-polystyrene blend film. *J. Mater. Sci. Mater. Electron.* **2022**, *33*, 25174–25185. [CrossRef]
4. El-naggar, A.M.; Alsaggaf, A.; Heiba, Z.K.; Kamal, A.M.; Aldhafiri, A.M.; Fatehmulla, A.; Mohamed, M.B. Exploring the structural, optical and electrical characteristics of PVA/PANi blends. *Opt. Mater.* **2023**, *139*, 113771. [CrossRef]
5. El-Naggar, A.M.; Heiba, Z.K.; Kamal, A.M.; Abd-Elkader, O.H.; Mohamed, M.B. Impact of ZnS/Mn on the Structure, Optical, and Electric Properties of PVC Polymer. *Polymers* **2023**, *15*, 2091. [CrossRef]
6. Badawi, A. Engineering the optical properties of PVA/PVP polymeric blend in situ using tin sulfide for optoelectronics. *Appl. Phys. A* **2020**, *126*, 335. [CrossRef]
7. El-naggar, A.M.; Heiba, Z.K.; Kamal, A.M.; Lakshminarayana, G.; Abd-Elkader, O.H.; Mohamed, M.B. Preparation of PVA/CMC/PVP blended polymer loaded with ZnS1-xCux; investigation of structural and linear/nonlinear optical properties. *Opt. Mater.* **2022**, *133*, 113066. [CrossRef]
8. Zyoud, S.H.; AlAbdulaal, T.H.; Almoadi, A.; Alqahtani, M.S.; Harraz, F.A.; Al-Assiri, M.S.; Yahia, I.S.; Zahran, H.Y.; Mohammed, M.I.; Abdel-wahab, M.S. Linear/Nonlinear Optical Characteristics of ZnO-Doped PVA/PVP Polymeric Films for Electronic and Optical Limiting Applications. *Crystals* **2023**, *13*, 608. [CrossRef]

9. Taha, T.A.; Alzara, M.A.A. Synthesis, thermal and dielectric performance of PVA-$SrTiO_3$ polymer nanocomposites. *J. Mol. Struct.* **2021**, *1238*, 130401. [CrossRef]
10. Rinaudo, M. Chitin and chitosan: Properties and applications. *Prog. Polym. Sci.* **2006**, *31*, 603–632. [CrossRef]
11. Abdelrazek, E.M.; Elashmawi, I.S.; Labeeb, S. Chitosan filler effects on the experimental characterization, spectroscopic investigation and thermal studies of PVA/PVP blend films. *Phys. B Condens. Matter* **2010**, *405*, 2021–2027. [CrossRef]
12. Alharthi, S.S.; Althobaiti, M.G.; Alkathiri, A.A.; Ali, E.E.; Badawi, A. Exploring the functional properties of PVP/PVA blend incorporated with non-stoichiometric SnS for optoelectronic devices. *J. Taibah Univ. Sci.* **2022**, *16*, 317–329. [CrossRef]
13. Alsulami, Q.A.; Rajeh, A. Modification and development in the microstructure of PVA/CMC-GO/Fe3O4 nanocomposites films as an application in energy storage devices and magnetic electronics industry. *Ceram. Int.* **2023**, *49*, 14399–14407. [CrossRef]
14. Rani, P.; Deshmukh, K.; Kadlec, J.; Krishna Karthik, T.V.; Khadheer Pasha, S.K. Dielectric properties of graphene/nano-Fe_2O_3 filled poly (vinyl alcohol)/Chitosan blends. *Mater. Chem. Phys.* **2023**, *295*, 126986. [CrossRef]
15. Pashameah, R.A.; El-Sharnouby, M.; El-Askary, A.; El-Morsy, M.A.; Ahmed, H.A.; Menazea, A.A. Optical, Structural, Electrical Characterization of (Polyvinyl Alcohol–Carboxymethyl Cellulose-Manganese Dioxide) Nanocomposite Fabricated via Laser Ablation. *J. Inorg. Organomet. Polym. Mater.* **2022**, *32*, 2863–2872. [CrossRef]
16. Norouzi, F.; Pourmadadi, M.; Yazdian, F.; Khoshmaram, K.; Mohammadnejad, J.; Sanati, M.H.; Chogan, F.; Rahdar, A.; Baino, F. PVA-Based Nanofibers Containing Chitosan Modified with Graphene Oxide and Carbon Quantum Dot-Doped TiO_2 Enhance Wound Healing in a Rat Model. *J. Funct. Biomater.* **2022**, *13*, 300. [CrossRef]
17. Venkataprasanna, K.S.; Prakash, J.; Vignesh, S.; Bharath, G.; Venkatesan, M.; Banat, F.; Sahabudeen, S.; Ramachandran, S.; Devanand Venkatasubbu, G. Fabrication of Chitosan/PVA/GO/CuO patch for potential wound healing application. *Int. J. Biol. Macromol.* **2020**, *143*, 744–762. [CrossRef]
18. Tauc, J. *Amorphous and Liquid Semiconductors*; Springer: Boston, MA, USA, 1974.
19. Badawi, A. Effect of the non-toxic Ag2S quantum dots size on their optical properties for environment-friendly applications. *Phys. E Low-Dimens. Syst. Nanostructures* **2019**, *109*, 107–113. [CrossRef]
20. El-naggar, A.M.; Heiba, Z.K.; Mohamed, M.B.; Kamal, A.M.; Lakshminarayana, G.; Abd-Elkader, O.H. Effect of MnS/ZnS nanocomposite on the structural, linear and nonlinear optical properties of PVA/CMC blended polymer. *Opt. Mater.* **2022**, *128*, 112379. [CrossRef]
21. Shamekh, A.M.A.; Shaalan, N.M.; Hanafy, T.A.; Rashad, M. Linear/nonlinear optical properties of functional inorganic MgO nano-filler in PVA transparent polymer for flexible optoelectronic devices. *Phys. B Condens. Matter* **2023**, *651*, 414617. [CrossRef]
22. Wemple, S.H.; DiDomenico, M. Behavior of the Electronic Dielectric Constant in Covalent and Ionic Materials. *Phys. Rev. B* **1971**, *3*, 1338–1351. [CrossRef]
23. Palik, E.D. *Handbook of Optical Constants of Solids*; Academic Press Handbook: New York, NY, USA, 1985.
24. Abdelrazek, E.M.; Ragab, H.M. Spectroscopic and dielectric study of iodine chloride doped PVA/PVP blend. *Indian J. Phys.* **2015**, *89*, 577–585. [CrossRef]
25. Elhosiny Ali, H.; Algarni, H.; Yahia, I.S.; Khairy, Y. Optical absorption and linear/nonlinear parameters of polyvinyl alcohol films doped by fullerene. *Chin. J. Phys.* **2021**, *72*, 270–285. [CrossRef]
26. El-naggar, A.M.; Heiba, Z.K.; Mohamed, M.B.; Kamal, A.M.; Osman, M.M.; Albassam, A.A.; Lakshminarayana, G. Improvement of the optical characteristics of PVA/PVP blend with different concentrations of SnS2/Fe. *J. Vinyl Addit. Technol.* **2022**, *28*, 82–93. [CrossRef]
27. Ismail, M.S.; Elamin, A.A.; Abdel-Wahab, F.; Elbashar, Y.H.; Mahasen, M.M. Improving the refractive index by engineering PbS/PVA nano polymer composite for optoelectronic applications. *Opt. Mater.* **2022**, *131*, 112639. [CrossRef]
28. Soliman, T.S.; Zaki, M.F.; Hessien, M.M.; Elkalashy, S.I. The structure and optical properties of PVA-BaTiO3 nanocomposite films. *Opt. Mater.* **2021**, *111*, 110648. [CrossRef]
29. Elango, M.; Deepa, M.; Subramanian, R.; Musthafa, A.M. Synthesis, Characterization, and Antibacterial Activity of Polyindole/Ag–Cuo Nanocomposites by Reflux Condensation Method. *Polym. -Plast. Technol. Eng.* **2018**, *57*, 1440–1451. [CrossRef]
30. Abdullah, O.G.; Aziz, S.B.; Rasheed, M.A. Structural and optical characterization of PVA:KMnO4 based solid polymer electrolyte. *Results Phys.* **2016**, *6*, 1103–1108. [CrossRef]
31. Alharthi, S.S.; Alzahrani, A.; Razvi, M.A.N.; Badawi, A.; Althobaiti, M.G. Spectroscopic and Electrical Properties of Ag_2S/PVA Nanocomposite Films for Visible-Light Optoelectronic Devices. *J. Inorg. Organomet. Polym. Mater.* **2020**, *30*, 3878–3885. [CrossRef]
32. Gu, Y.; Tang, L.; Guo, X.; Xiang, J.; Seng Teng, K.; Ping Lau, S. Preparation and photoelectric properties of cadmium sulfide quantum dots. *Chin. Phys. B* **2019**, *28*, 047803. [CrossRef]
33. Zidan, H.M.; Abdelrazek, E.M.; Abdelghany, A.M.; Tarabiah, A.E. Characterization and some physical studies of PVA/PVP filled with MWCNTs. *J. Mater. Res. Technol.* **2019**, *8*, 904–913. [CrossRef]
34. Al-Hakimi, A.N.; Asnag, G.M.; Alminderej, F.; Alhagri, I.A.; Al-Hazmy, S.M.; Qahtan, T.F. Enhancing the Structural, Optical, Thermal, and Electrical Properties of PVA Filled with Mixed Nanoparticles (TiO_2/Cu). *Crystals* **2023**, *13*, 135. [CrossRef]
35. Bdewi, S.F.; Abdullah, O.G.; Aziz, B.K.; Mutar, A.A.R. Synthesis, Structural and Optical Characterization of MgO Nanocrystalline Embedded in PVA Matrix. *J. Inorg. Organomet. Polym. Mater.* **2016**, *26*, 326–334. [CrossRef]

36. Omkaram, I.; Sreekanth Chakradhar, R.P.; Lakshmana Rao, J. EPR, optical, infrared and Raman studies of VO^{2+} ions in polyvinylalcohol films. *Phys. B Condens. Matter* **2007**, *388*, 318–325. [CrossRef]
37. Al-Muntaser, A.A.; Pashameah, R.A.; Alzahrani, E.; AlSubhi, S.A.; Tarabiah, A.E. Tuning structural, optical, and dispersion functions of polystyrene via addition of meso-tetraphenylporphine manganese (III) chloride towards optoelectronic applications. *Opt. Mater.* **2023**, *135*, 113333. [CrossRef]
38. Singh, P.K.; Kumar, P.; Hussain, M.; Das, A.K.; Nayak, G.C. Synthesis and characterization of CuO nanoparticles using strong base electrolyte through electrochemical discharge process. *Bull. Mater. Sci.* **2016**, *39*, 469–478. [CrossRef]
39. Ponnar, M.; Thangamani, C.; Monisha, P.; Gomathi, S.S.; Pushpanathan, K. Influence of Ce doping on CuO nanoparticles synthesized by microwave irradiation method. *Appl. Surf. Sci.* **2018**, *449*, 132–143. [CrossRef]
40. Kumar, N.; Parui, S.S.; Limbu, S.; Mahato, D.K.; Tiwari, N.; Chauhan, R.N. Structural and optical properties of sol–gel derived CuO and Cu2O nanoparticles. *Mater. Today Proc.* **2021**, *41*, 237–241. [CrossRef]
41. Chang, Y.-N. Fourier Transform Infrared (FTIR) Analysis of Copper Oxide Thin Films Prepared by Metal Organic Chemical Vapor Deposition (MOCVD). *MRS Online Proc. Libr. (OPL)* **2011**, *293*, 443. [CrossRef]
42. Badawi, A.; Alharthi, S.S. Controlling the optical and mechanical properties of polyvinyl alcohol using Ag_2S semiconductor for environmentally friendly applications. *Mater. Sci. Semicond. Process.* **2020**, *116*, 105139. [CrossRef]
43. Badawi, A.; Alharthi, S.S. The optical, electrical and mechanical performance of metal oxides incorporated PVA/rGO blend: Effect of metal oxide type. *Appl. Phys. A* **2022**, *128*, 328. [CrossRef]
44. Heiba, Z.K.; Mohamed, M.B.; Badawi, A.; Alhazime, A.A. The role of Cd0.9Mg0.1S nanofillers on the structural, optical, and dielectric properties of PVA/CMC polymeric blend. *Chem. Phys. Lett.* **2021**, *770*, 138460. [CrossRef]
45. Bosigo, R.; Lepodise, L.M.; Kuvarega, A.; Muiva, C. Hydrothermal synthesis of CuO and CeO_2/CuO nanostructures: Spectroscopic and temperature dependent electrical properties. *J. Mater. Sci. Mater. Electron.* **2021**, *32*, 7136–7152. [CrossRef]
46. Alhazime, A.A. Effect of Nano CuO Doping on Structural, Thermal and Optical Properties of PVA/PEG Blend. *J. Inorg. Organomet. Polym. Mater.* **2020**, *30*, 4459–4467. [CrossRef]
47. Badawi, A.; Alharthi, S.S.; Althobaiti, M.G.; Alharbi, A.N. The effect of iron oxide content on the structural and optical parameters of polyvinyl alcohol/graphene nanocomposite films. *J. Vinyl Addit. Technol.* **2022**, *28*, 235–246. [CrossRef]
48. Abdullah, O.G.; Aziz, S.B.; Rasheed, M.A. Effect of silicon powder on the optical characterization of Poly(methyl methacrylate) polymer composites. *J. Mater. Sci. Mater. Electron.* **2017**, *28*, 4513–4520. [CrossRef]
49. Aslam, M.; Kalyar, M.A.; Raza, Z.A. Fabrication of nano-CuO-loaded PVA composite films with enhanced optomechanical properties. *Polym. Bull.* **2021**, *78*, 1551–1571. [CrossRef]
50. Mohamed, S.H.; Drese, R. Structural and optical properties of direct current sputtered zinc aluminum oxides with a high Al concentration. *Thin Solid Film.* **2006**, *513*, 64–71. [CrossRef]
51. Dhatarwal, P.; Sengwa, R.J. Investigation on the optical properties of (PVP/PVA)/Al_2O_3 nanocomposite films for green disposable optoelectronics. *Phys. B Condens. Matter* **2021**, *613*, 412989. [CrossRef]
52. Abdulwahid, R.T.; Abdullah, O.G.; Aziz, S.B.; Hussein, S.A.; Muhammad, F.F.; Yahya, M.Y. The study of structural and optical properties of PVA:PbO2 based solid polymer nanocomposites. *J. Mater. Sci. Mater. Electron.* **2016**, *27*, 12112–12118. [CrossRef]
53. Elhosiny Ali, H.; Khairy, Y. Tailoring structure, nonlinear/linear optical, and dielectric properties of PVA/PVP film by spinel LiMn2O4 nanoparticles. *Chin. J. Phys.* **2022**, *78*, 27–43. [CrossRef]
54. Alharthi, S.S.; Badawi, A. Tailoring the linear and nonlinear optical characteristics of PVA/PVP polymeric blend using Co0.9Cu0.1S nanoparticles for optical and photonic applications. *Opt. Mater.* **2022**, *127*, 112255. [CrossRef]
55. Badawi, A.; Alharthi, S.S.; Assaedi, H.; Alharbi, A.N.; Althobaiti, M.G. Cd0.9Co0.1S nanostructures concentration study on the structural and optical properties of SWCNTs/PVA blend. *Chem. Phys. Lett.* **2021**, *775*, 138701. [CrossRef]
56. Malik, Z.; Khattak, A.; Alahmadi, A.A.; Butt, S.U. Development and Investigation of High Performance PVA/NiO and PVA/CuO Nanocomposites with Improved Physical, Dielectric and Mechanical Properties. *Materials* **2022**, *15*, 5154. [CrossRef] [PubMed]
57. Najm, S.S. Doping effect on the optical properties of(PVA: ZNO) nanocomposites. *Mater. Today Proc.* **2022**, *61*, 632–635. [CrossRef]
58. Darwesh, A.H.A.; Aziz, S.B.; Hussen, S.A. Insights into optical band gap identification in polymer composite films based on PVA with enhanced optical properties: Structural and optical characteristics. *Opt. Mater.* **2022**, *133*, 113007. [CrossRef]
59. El-naggar, A.M.; Heiba, Z.K.; Mohamed, M.B.; Kamal, A.M.; Lakshminarayana, G. PVA/PVP/PEG polymeric blend loaded with nano-Zn0.75−xFexCd0.25S: Effect of iron concentration on the optical characteristics. *Appl. Phys. A* **2022**, *128*, 220. [CrossRef]
60. Alshammari, A.H.; Alshammari, M.; Ibrahim, M.; Alshammari, K.; Taha, T.A.M. New Hybrid PVC/PVP Polymer Blend Modified with Er_2O_3 Nanoparticles for Optoelectronic Applications. *Polymers* **2023**, *15*, 684. [CrossRef] [PubMed]
61. Alhazime, A.A.; Mohamed, M.B.; Abdel-Kader, M.H. Effect of Zn1−xMgxS Doping on Structural, Thermal and Optical Properties of PVA. *J. Inorg. Organomet. Polym. Mater.* **2019**, *29*, 436–443. [CrossRef]
62. Abouhaswa, A.S.; Taha, T.A. Tailoring the optical and dielectric properties of PVC/CuO nanocomposites. *Polym. Bull.* **2020**, *77*, 6005–6016. [CrossRef]
63. Suresh, B.; Ramachandran, S.; Shanmugam, G. Effect of Cerium dopant on third-order nonlinear optical properties of CdS/PEG self-standing nanocomposite films. *Opt. Mater.* **2023**, *135*, 113299. [CrossRef]

64. Erken, O. Effect of cycle numbers on the structural, linear and nonlinear optical properties in Fe_2O_3 thin films deposited by SILAR method. *Curr. Appl. Phys.* **2022**, *34*, 7–18. [CrossRef]
65. Elhosiny Ali, H.; Ganesh, V.; Haritha, L.; Aboraia, A.M.; Hegazy, H.H.; Butova, V.; Soldatov, A.V.; Algarni, H.; Guda, A.; Zahran, H.Y.; et al. Kramers-Kronig analysis of the optical linearity and nonlinearity of nanostructured Ga-doped ZnO thin films. *Opt. Laser Technol.* **2021**, *135*, 106691. [CrossRef]